Structural Engineering and Mechanics, *Vol. 68, No. 6 (2018) 677-689*
DOI: https://doi.org/10.12989/sem.2018.68.6.677

Seismic fragility assessment of self-centering RC frame structures considering maximum and residual deformations

Lu-Xi Li[1], Hong-Nan Li[1, 2] and Chao Li*[1]

[1]State Key Lab. of Coastal Offshore Engineering, Faculty of Infrastructure Engineering, Dalian University of Technology, Dalian, China
[2]School of Civil Engineering, Shenyang Jianzhu University, Shenyang, China

(Received August 17, 2018, Revised October 31, 2018, Accepted November 7, 2018)

Abstract. Residual deformation is a crucial index that should be paid special attention in the performance-based seismic analyses of reinforced concrete (RC) structures. Owing to their superior re-centering capacity under earthquake excitations, the post-tensioned self-centering (PTSC) RC frames have been proposed and developed for engineering application during the past few decades. This paper presents a comprehensive assessment on the seismic fragility of a PTSC frame by simultaneously considering maximum and residual deformations. Bivariate limit states are defined according to the pushover analyses for maximum deformations and empirical judgments for residual deformations. Incremental Dynamic Analyses (IDA) are conducted to derive the probability of exceeding predefined limit states at specific ground motion intensities. Seismic performance of the PTSC frame is compared with that of a conventional monolithic RC frame. The results show that, taking a synthetical consideration of maximum and residual deformations, the PTSC frame surpasses the monolithic frame in resisting most damage states, but is more vulnerable to ground motions with large intensities.

Keywords: self-centering; RC frame; joint seismic fragility; bivariate limit states; maximum deformations; residual deformations

1. Introduction

Reinforced concrete frames constitute a major part of modern building structures and their seismic performances have always been attracting the attentions of structural engineers and academic researchers. Early on, the structural analyses of RC frames mainly concentrated on preventing structural failure and ensuring life safety. However, significant social and economic impacts of recent earthquakes have aroused awareness of the fact that, even though structural collapse may be generally prevented, enormous property loss could be caused due to the different degrees of structural damage (Muguruma *et al.* 1995, Eguchi *et al.* 1998, Saatcioglu *et al.* 2001, Ghosh and Cleland 2012). Therefore, the Performance-Based Earthquake Engineering (PBEE) has been proposed to control the seismic risk and economic loss by associating the structural damage with multiple performance levels (ATC 1996, 1997, 2000, Cornell and Krawinkler 2000).

In the framework of PBEE, the structural seismic performance is usually evaluated in terms of maximum displacement responses, such as the maximum roof displacement or maximum interstory drift. However, in addition to peak deformations, residual deformations also play an important role in the seismic performance of a building, which can leave a structure in an incipient collapse state and impair its capability to resist aftershocks (Luco *et al.* 2004, Mackie and Stojadinovic 2004). Moreover, the residual deformation is a critical index to measure the difficulties, costs, and feasibility of repairing damaged structures after earthquake events. For instance, after the 1985 Michoacan earthquake, several dozen damaged RC buildings in Mexico City had to be demolished due to the large permanent drifts that made them technically difficult to be straightened and repaired (Rosenblueth and Meli 1986). The 1995 Kobe earthquake also left 240,000 buildings requiring decision on the feasibility of repair versus demolition. Accordingly, special emphasis should be placed on residual deformations in conjunction with maximum displacement responses when assessing the seismic performance of a RC frame structure.

The concept of self-centering (SC) was firstly put forward in the Precast Seismic Structural Systems (PRESSS) Research Program during the 1990s (Priestley 1991, Nakaki and Englekirk 1991). Innovative attempts were made to use unbonded post-tensioned (PT) tendons to compress precast concrete beam and column members together to achieve lateral resistance. In this structural system, it is expected that the beams should act as rigid bodies and deformations mainly concentrate at the beam-to-column joints (El-Sheikh *et al.* 1999). A large amount of research investments have been conducted on the seismic performance of the beam-to-column connections (Cheok and Lew 1991, Priestley and Macrae 1996, Stanton 1997, Christopoulos *et al.* 2002, Morgen and Kurama 2004, Garlock 2005, Chou *et al.* 2006, Song *et al.* 2014, Zhang *et al.* 2016). Some researchers experimentally explored the mechanical properties of the beam-to-column joints with unbonded PT tendons under cyclic loadings, and the test

*Corresponding author, Post-Doctoral Researcher
E-mail: chao.li@mail.dlut.edu.cn

Copyright © 2018 Techno-Press, Ltd.
http://www.techno-press.com/journals/sem&subpage=7
ISSN: 1225-4568 (Print), 1598-6217 (Online)

results demonstrated substantial strength and ductility, negligible residual deformations while relatively small energy dissipation of the connections (Cheok and Lew 1991, Priestley and Macrae 1996). To increase the structural energy dissipation, various damping devices have been developed and appended to the SC structures (Stanton 1997, Christopoulos *et al.* 2002, Morgen and Kurama 2004, Garlock 2005, Chou *et al.* 2006, Song *et al.* 2014). Among these, the top-and-seat angles have been validated as a simple but effective provider of supplemental energy dissipation (Garlock 2005, Lu *et al.* 2015).

In addition to the study on the SC beam-to-column connections, the structural performance (Morgen and Kurama 2008, Chou and Chen 2010, Lin *et al.* 2013a, Lin *et al.* 2013b, Lu *et al.* 2015, Song 2016, Qiu and Zhu 2017, Rahgozar *et al.* 2017, Fang *et al.* 2018, Tian and Qiu 2018) and design approaches (Morgen and Kurama 2007, Garlock *et al.* 2007, Chou and Chen 2011) of the SC frame structures have been investigated. Moreover, some design criteria have been issued based on the extensive research and practical activities (ACI Innovation Task Group 1 2001, NZS 2006). Guo *et al.* (2016) conducted a series of quasi-static cyclic tests on two SC concrete frames and a conventional RC frame. The test observations showed that the frame with SC beam-to-column connections and fixed column bases sustained similar crack pattern of columns while effectively prevented the damage at beam-to-column joints as compared with the conventional RC frame. Moreover, comparable lateral strength and deformation capacity but smaller energy dissipation of the SC frame were demonstrated. Lu *et al.* (2015) and Cui *et al.* (2017) carried out shaking table tests of SC concrete frames, in which satisfactory seismic performance and self-centering capacity were observed. Chou and Chen (2011) performed shaking table tests of a SC frame comprising of PT concrete-filled tube columns and PT steel beams. Although excessive maximum structural responses were observed under the Chi-Chi earthquake recording with a PGA of 1.87 g, the good self-centering capacity of the specimen was demonstrated with a residual drift of only 0.01%. As a complement of experimental investigations, numerical models with typical gap opening of beam-to-column joints and SC behavior of the structures have also been developed (Kim and Christopoulos 2009, Song 2014, Lu *et al.* 2015). The existing studies have validated the availability and effectiveness of the SC frame system and its superior capacity in eliminating residual deformations. However, a comprehensive evaluation of the seismic performance of SC frame structures with inclusion of both structural maximum and residual responses is very scarce.

Seismic fragility expresses the probability for a structure to exceed various performance levels, in other words, the possibility of suffering different degrees of damage under a certain level of ground motion intensity (Elnashait *et al.* 2004, Erberik and Elnashai 2004, Li *et al.* 2016, Li *et al.* 2018). In the seismic fragility analyses, structural capacities, represented by the defined limit states of different performance levels, are compared with structural seismic demands under different intensities of seismic inputs. In recent years, a lot of research efforts have been devoted on the development of seismic fragility methodology for various types of engineering structures (Kwon and Elnashai 2006, Ellingwood *et al.* 2007, Rota *et al.* 2010, Borekci and Kircil 2011, Kang and Lee 2016, Waseem and Spacone 2017). However, very little attention has been paid to the seismic fragility of SC structures. To the best knowledge of the authors, only few papers (Kammula *et al.* 2014, Guo *et al.* 2015) studied the seismic fragility of SC steel structures, in which only the maximum deformation is taken into account when evaluating the performance levels and seismic demands. As discussed above, the most significant characteristic of a SC structure is the superior self-centering capability to control residual deformations after earthquakes. Thereby, simultaneously considering the seismic demands of maximum and residual deformations is vital for a comprehensive seismic fragility assessment of SC frames. Christopoulos *et al.* (2003) and Pampanin *et al.* (2003) employed the residual deformation damage index as an additional indicator for the seismic performance levels of RC structures. A three-dimensional performance matrix comprising performance levels defined by a combination of maximum and residual deformations along with seismic excitation levels was developed by Pampanin *et al.* (2002). Uma *et al.* (2010) further extended the framework with the probabilistic approach and assessed the seismic fragility of RC frame structures. More recently, Shrestha *et al.* (2016) applied this probability framework to study the seismic performance of SMA-reinforced bridge piers. As a new type of structure, the seismic performance of SC frames should be adequately evaluated and compared to conventional RC frame structures. Yet, a direct comparison of the seismic fragilities between the conventional RC frame and the comparable SC frame with inclusion of both maximum and residual structural deformations cannot be found in available literature.

In this paper, a comprehensive seismic performance assessment of a PT self-centering (PTSC) reinforced concrete frame with the simultaneous consideration of maximum and residual responses is conducted. Comparisons are made with a conventional monolithic RC frame, which possesses the identical structural configuration and design criteria with the PTSC frame. The joint seismic fragility curves are developed to represent the probabilities of seismic demands (expressed by the combined maximum-residual deformations) exceeding the predefined bivariate limit states. Considering the characteristic difference between the conventional RC frame and the PTSC frame, the bivariate limit states are defined according to the respective properties of these two frames. In total 30 real earthquake records are selected for the Incremental Dynamic Analyses (IDA). The seismic responses and fragilities of these two frame structures are compared. The advantages and disadvantages of the PTSC system in resisting earthquake loadings against the monolithic RC frame are discussed in detail.

2. Joint fragility function methodology

Fragility function describes the conditional probability of attaining or exceeding a specified damage state for a set of ground motion intensity levels. The problem can be disaggregated into two interim probabilistic models, namely the probabilistic seismic demand model (PSDM) and the probabilistic damage model. The PSDM relates the input ground motions to the structural responses by calculating the probabilistic distribution of engineering demand parameters (EDPs) conditioned on intensity measures (IMs). Subsequently, the EDPs are compared with the limit states (LSs) corresponding to various performance levels (PLs) to derive the probability of reaching corresponding damage states (DSs). The fragility function can be expressed as

$$P\left[DS\left|IM\right.\right]=\int P\left[DS\left|EDP\right.\right]\left|dP\left[EDP\left|IM\right.\right]\right. \tag{1}$$

The seismic failure of a structure is mainly governed by the displacement response, and the interstory drift is generally used as the EDP indicator and DS definition for RC frames. Here, a bivariate deformation index that contains both of maximum drifts (MDs) and residual drifts (RDs) instead of a single indicator (MD in most previous studies) is adopted.

The IDA (Vamvatsikos and Cornell 2002) is performed to develop the PSDM. Pairs of EDPs corresponding to the MDs and RDs can be obtained through nonlinear dynamic time history analyses with input ground motions scaled to various IM levels. A bivariate lognormal distribution is assumed as the joint probability density function (JPDF) of MD and RD pairs at a given IM (Uma *et al.* 2010). The JPDF for the bivariate lognormal distribution of MD (X) and RD (Y) can be expressed as

$$f_{X,Y}(x,y)=\frac{1}{2xy\pi\zeta_X\zeta_Y\sqrt{1-\rho^2}}\cdot\exp\left\{-\frac{1}{2\left(1-\rho^2\right)}\left[\frac{\left(\log x-\lambda_X\right)^2}{\zeta_X^2}-\frac{2\rho\left(\log x-\lambda_X\right)\left(\log y-\lambda_Y\right)}{\zeta_X\zeta_Y}+\frac{\left(\log y-\lambda_Y\right)^2}{\zeta_Y^2}\right]\right\} \tag{2}$$

where λ_X , λ_Y and ζ_X , ζ_Y are the lognormal mean values and standard deviations of X and Y, respectively; and ρ denotes the linear correlation coefficient between the two variables.

Christopoulos *et al.* (2003) proposed a performance matrix with inclusion of bivariate measures of MD and RD. As shown in Fig. 1(a), the elements in the table represent the joint PLs defined by pairs of LSs of MDs (columns of the table) and RDs (rows of the table). PL_{ij} corresponds to a performance state that lies in the domain limited by the ith LS of MD (index i) coupled with the jth LS of RD (index j). Due to the inadequacy of well-calibrated stochastic LSs of PLs (especially for residual deformations), the deterministic LSs are used for both variables in this study. At each IM, the probability of being in PL_{ij} can be obtained by conducting a double integration over the aforementioned PDF in the interval from zero to the limits of MD_i and RD_j. Furthermore, the complement of this probability represents the likelihood of exceeding PL_{ij}, namely the seismic fragility for the corresponding damage state (DS_{ij}) under the specified IM.

Note that the assumption of the bivariate lognormal distribution is only applicable when the structure does not collapse in this study, for the reasons that will be explained in the following part. The fragility function for a structure that is not collapsed can thus be written by

$$P\left(DS_{ij}\left|NC\right.\right)=1-P\left(PL_{ij}\left|NC\right.\right) \tag{3}$$

$$P\left(PL_{ij}\left|NC\right.\right)=\int_0^{MD_i}\int_0^{RD_j}f_{X,Y}\left(x,y\right)dxdy \tag{4}$$

where $P\left(PL_{ij}\left|NC\right.\right)$ and $P\left(DS_{ij}\left|NC\right.\right)$ respectively denote the probabilities of being within PL_{ij} and reaching DS_{ij} conditioned that the structure does not collapse. An explicit illustration of this fragility analysis process is shown in Fig. 1.

When subjected to strong seismic ground motions, buildings may become instable due to structural element deterioration and P-Δ effects, and collapse will take place as the ultimate state. In the collapse state, the dispersion of MDs is too large to be included in the statistical analysis, and the consideration of RDs becomes insignificant. The assumption of bivariate lognormal distribution is not reasonable any more. Therefore, the probability of collapse is calculated separately and incorporated in the fragility analysis using the total probability theorem as briefed below

$$P\left(DS_{ij}\left|IM\right.\right)=P\left(DS_{ij}\left|NC\right.\right)\cdot P\left(NC\left|IM\right.\right)+P\left(C\left|IM\right.\right) \tag{5}$$

$$P\left(C\left|IM\right.\right)=\frac{n}{N} \tag{6}$$

$$P\left(NC\left|IM\right.\right)=1-P\left(C\left|IM\right.\right) \tag{7}$$

where $P\left(C\left|IM\right.\right)$ refers to the probability of collapse at each IM, which is defined as the ratio of the number of ground motions that induce collapse (n) to the total number of input motions (N); $P\left(NC\left|IM\right.\right)$ is the possibility for the structure retaining in the un-collapsed condition, which equals to the complementary to $P\left(C\left|IM\right.\right)$. $P\left(DS_{ij}\left|NC\right.\right)$ can be calculated according to Eqs. (3) and (4).

According to the method presented above, the seismic motion inputs that lead to structural collapse are firstly extracted at each IM level. $P\left(C\left|IM\right.\right)$ and $P\left(NC\left|IM\right.\right)$ are calculated according to Eqs. (6)-(7). For the rest ground motion inputs, the statistical parameters of MDs and RDs are calculated to construct the JPDF of the bivariate lognormal distribution defined by Eq. (2). Subsequently, the probability of exceeding a certain PL is calculated using Eqs. (3)-(4). The seismic fragility with respect to a specified DS can be finally obtained following Eq. (5).

3. Structural design and numerical modeling

In this section, a PTSC frame and a conventional monolithic RC frame are designed to compare the seismic performance of these two frame structures. The structural configurations and design criteria are set to be identical so that the structure type is the only difference between two frames. Detailed descriptions of the mechanical properties of the PTSC connections, along with the design and

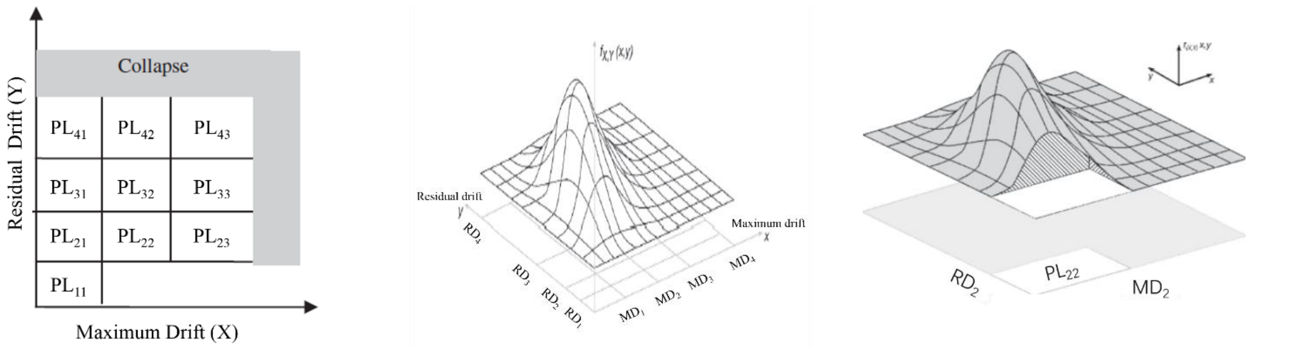

(a) (b) (c)

Fig. 1 (a) Performance table considering the combination of MDs and RDs (Christopoulos *et al.* 2003), (b) Joint probability density function and bivariant performance table (Uma *et al.* 2010), and (c) Probability of reaching a specified DS (Uma *et al.* 2010)

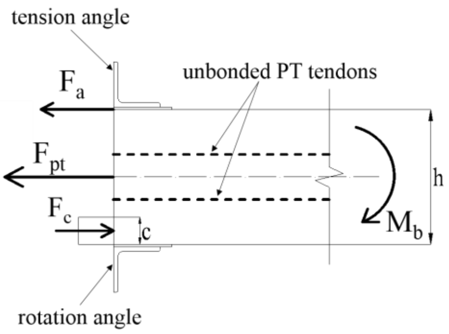

Fig. 2 Schematic diagram of forces at a beam-to-column interface

modeling of two frames are introduced in detail.

3.1 Behavior of PTSC connections

This paper focuses on the self-centering RC frame consisting of unbonded PT tendons through the precast beams to compress them to columns and using the top-and-seat angles at the beam ends as energy dissipation devices. The beam-to-column connections behave elastically as rigid joints until decompression occurs at the top or bottom flange of the beam ends. After decompression, gaps open at the beam-to-column interfaces. Taking the case of a clockwise bending moment M_b at the beam end as an example, Fig. 2 shows the schematic diagram of forces at a beam-to-column interface after gap opening. In this case, the top angle is referred to as the tension angle and deforms to provide the tension force F_a. The location of F_a is considered at the beam edge for simplification. The bottom angle can be treated as the rotation angle which does not provide any reaction force in the horizontal direction. F_{pt} denotes the resultant force of the PT tendons and F_c is the concrete compressive force. According to the equilibrium of forces, the following equations can be obtained

$$F_c = F_{pt} + F_a \tag{8}$$

$$M_b = M_{pt} + M_a \tag{9}$$

where M_{pt} and M_a respectively denote the contributions of PT tendons and the angle to the moment strength, which can be written by

$$M_{pt} = F_{pt} \cdot \frac{h-c}{2} \tag{10}$$

$$M_a = F_a \cdot \left(h - \frac{c}{2} \right) \tag{11}$$

where h is the beam depth and c is the depth of the assumed uniform concrete compressive stress block, as illustrated in Fig. 2. It should be noted that the vertical shear force at the beam end is resisted by the friction at the compressed beam-to-column interface, therefore it is not incorporated in the force analysis.

3.2 Structural configuration and design

The prototype structure of two frames is a 6-story RC building with a symmetric plan layout, as shown in Fig. 3(a). The double-symmetry plan arrangement enables the use of a two-dimensional frame model in the structural seismic response analysis. The elevation of the three-bay frame is shown in Fig. 3(b), the span length is 6 m and the story height is 3.6 m.

The monolithic frame is firstly designed according to the Chinese codes (National Standards of the People's Republic of China 2010a, b). The compressive strength of concrete is 23.4 MPa and the tensile strength of reinforcement bars is 400 MPa. The cross sections and reinforcement details of the beams and columns are shown in Figs. 3(c)-(e). To conduct direct comparisons of the seismic performance, the PTSC frame is designed using the same seismic design criteria. Identical cross section dimensions are employed to acquire a similar initial structural stiffness to that of the monolithic frame. Besides, the two frames are designed to have similar lateral strength. The reinforcements in the columns of PTSC frame are consistent with those of the monolithic frame. The required areas of PT tendons and angle sizes are determined by assuming that the nominal moment strengths of corresponding beam ends are the same for these two frames.

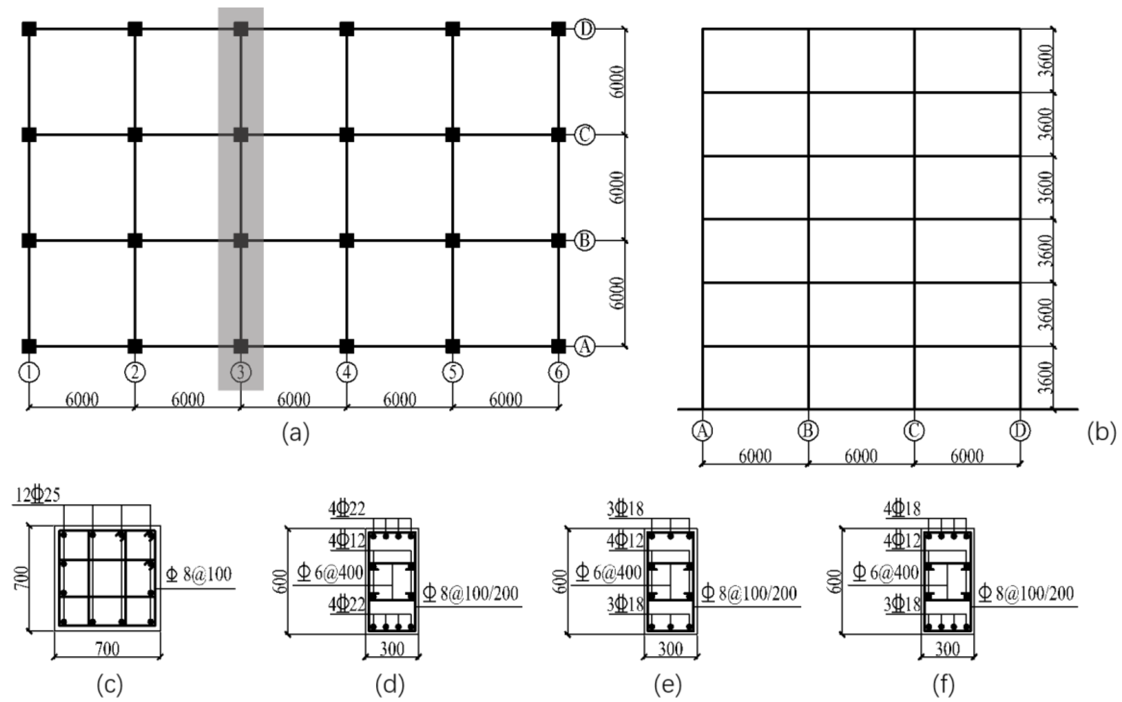

Fig. 3 Structural configurations. (a) plan of the prototype structure, (b) elevation of the prototype structure, (c) columns, (d) beams of 1-5th floors of the monolithic frame, (e) beams of the top floor of the monolithic frame, and (f) beams of the PTSC frame (unit: mm)

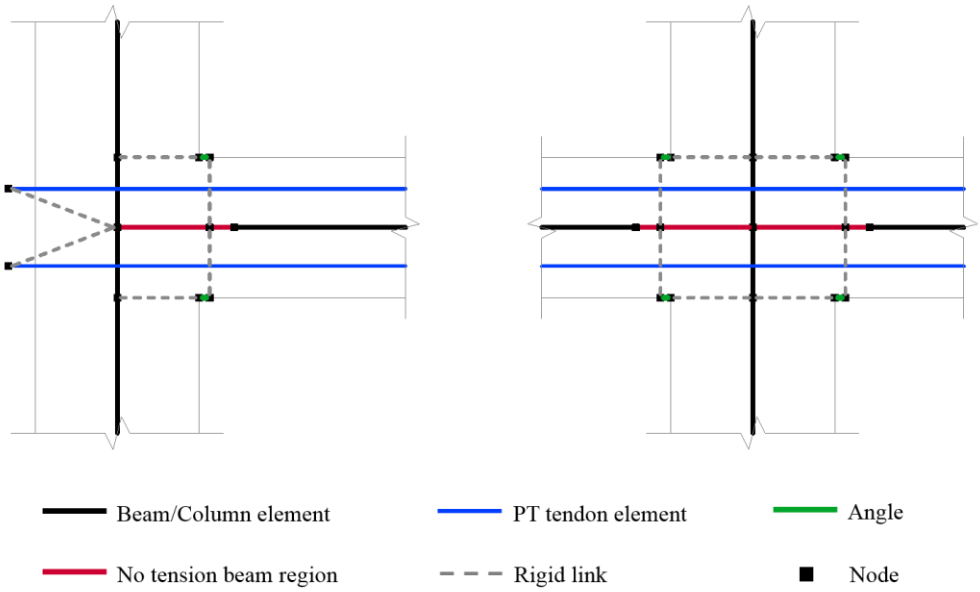

Fig. 4 Modeling of beam-to-column joints of the PTSC frame

The bending moment at the monolithic beam ends are calculated based on the reinforcement arrangement and assigned as M_b in Eq. (9). The forces provided by the PT tendon (F_{pt}) and angles (F_a) are respectively calculated according to the corresponding equations. According to Morgen and Kurama (2007), the ratio of the design damper moment to the beam end moment equals to the relative energy dissipation ratio β, which is defined in ACI T1.1-01 (ACI Innovation Task Group 1 2001) and should be no less than 0.125. Moreover, this ratio should not surpass 0.5 to maintain the self-centering behavior. Therefore, the contribution of angles to the total moment strength is set to be 0.25 to acquire sufficient energy dissipation while preserving the self-centering ability herein. The cross-sectional area and design initial stress of the PT tendons are 1680 mm^2 and 834 MPa for the beams of the 1-5th floor, while the corresponding values are 840 mm^2 and 536 MPa for the beams of the top floor. The yield strength of PT tendon is 1680 MPa, which is designed not to be reached to keep the tendons in the elastic range during the earthquake excitations. L200×200×20 and L140×140×12 angles are employed for the beam-to-column joints of the 1-5th floors

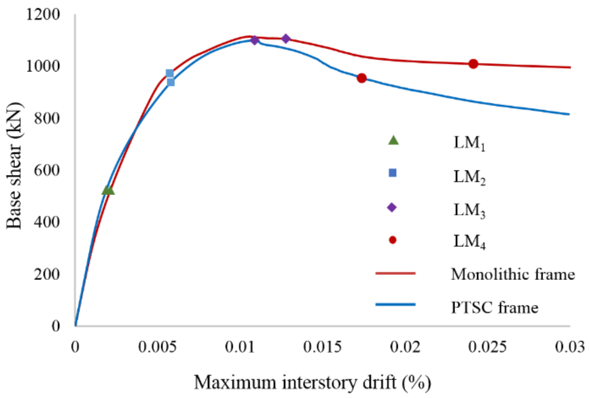

Fig. 5 Pushover curves and limit states based on maximum drifts

Table 1 Limit states based on maximum drifts

Maximum drift (%)	LM_1	LM_2	LM_3	LM_4
Monolithic frame	0.18%	0.57%	1.33%	2.43%
PTSC frame	0.17%	0.57%	1.11%	1.76%

and top floor, respectively. The yield strength of angles is 235 MPa. Since the seismic forces are mainly burdened by the PT tendons and angles, the longitudinal mild reinforcements in the precast beams are merely assigned to satisfy the constructional reinforcement ratio, as shown in Fig. 3(f).

3.3 Structural modeling

The finite element (FE) models of two kinds of frames are developed using the OpenSees platform (Mckenna and Fenves 2013). The monolithic frame is modeled using the nonlinear beam-column elements with fiber sections, which consist of a number of fibers that represent the cover concrete, reinforcing steels and the core concrete, respectively. The uniaxial material Concrete02 in the OpenSees is employed to simulate the cover and core concrete; while the reinforcements are modeled by the uniaxial material Steel02.

The FE models for the beam-to-column joints of the PTSC frame are shown in Fig. 4. The nonlinear beam-column elements are used to simulate the beams and columns. The unbonded PT tendons are modeled by the truss elements parallel to the beam elements. The Steel02 material model with initial stress values is assigned to the truss elements. The rigid links are used to tie the end nodes of truss elements to the column element nodes. The gap opening behavior at the beam-to-column interface is the most significant characteristic that distinguishes PTSC frame from the monolithic counterpart. When the pre-compressive stress at the marginal fibers of the beam end section is eliminated, the beam starts to separate from the column and gap opening occurs. The compressive zone of the contact surface decreases as the opening increases. Because the beam-to-column interface has no tensile capacity, the concrete and reinforcement materials without tensile capacity should be utilized to simulate the beam elements adjacent to the interface region. To achieve this goal, the uniaxial material Concrete01 without tensile strength is used to model the concrete and the uniaxial material Steel02 is combined with the MinMax material with an upper bound (tensile strength) of zero to simulate the reinforcing steels. The length of the no tension region of beam elements is assumed to be 400 mm according to Roh and Reinhorn (2009).

During the gap opening, the top-and-seat angles at the joints yield rapidly and begin to dissipate energy due to their nonlinear behavior. This behavior can be modeled by the nonlinear springs at the top and bottom flanges of the beam ends. Two node link elements are used to simulate the angles. One node of each element is linked to the column element and the other is connected to the beam element, as shown in Fig. 4. The Hysteretic material is assigned to the angle elements and the force-deformation relationship of the angles is specified according to the hysteretic rules proposed by Shen and Astaneh (2000).

4. Development of joint fragility curves

The joint seismic fragility analyses with simultaneous consideration of maximum and residual deformations are conducted for the PTSC and monolithic frames. Bivariate LSs based on the MDs and RDs are defined for the two frames. Incremental Dynamic Analyses (IDA) are performed to yield the seismic demands of the structural models under 30 selected real earthquake records.

4.1 Definition of bivariate limit states

Since the seismic behavior and failure mode of a structure are mainly governed by displacement responses, the LSs are defined to relate the deformations to the DSs. Definition of LSs plays an important role in the construction of the structural seismic fragility curves. Recent guidelines and design codes (ATC 1996, 1997, National Standards of the People's Republic of China 2010b) usually define the LSs with specified values based on the general performance of RC structures, regardless of the earthquake resistant capability of a specific structure. However, to achieve a rigorous seismic fragility analysis, it is necessary to define the LSs for each individual structure, especially for the special structural systems such as the PTSC structure, since the identification of LSs is highly dependent on the structural characteristics.

In this study, the LSs based on MDs (LMs) and RDs (LRs) are both defined in terms of the interstory drift ratio. For the LMs, pushover analyses are performed on the FE models of the two frames. In total four limit states are defined, i.e., LM_1, LM_2, LM_3 and LM_4. LM_1 refers to the first occurrence of crack in the columns, which indicates the termination of linear elastic behavior. LM_2 is identified with the equivalent yield point obtained from the pushover curve. LM_3 corresponds to the attainment of the maximum shear resistance. LM_4 is reached when the confined concrete in the columns attains its maximum compressive strain, which is also considered to be the initiation of structural collapse. The pushover curves of the monolithic

Table 2 Damage States based on the bivariate Limit States

LS based on MD	LS based on RD		
	LR_1	LR_2	LR_3
LM_1	DS_{11}	DS_{12}	DS_{13}
LM_2	DS_{21}	DS_{22}	DS_{23}
LM_3	DS_{31}	DS_{32}	DS_{33}
LM_4		DS_4	

frame and the PTSC frame are shown in Fig. 5. Four LMs of each frame are marked on the corresponding curve, respectively. It can be observed that the initial stiffness of PTSC frame is slightly higher than the monolithic frame benefiting from the prestressing force of the PT tendons, which is consistent with Stanton (1997). However, the stiffness of PTSC frame decreases faster and becomes lower than the monolithic counterpart after nonlinearity occurs. The interstory drift ratios with respect to LM_3 and LM_4 of the PTSC frame are smaller than those of the monolithic frame, especially for LM_4. A rapid strength deterioration is also observed for the PTSC frame after the maximum resistance is reached. This is due to the identical design details for the columns while different beam-to-column joints of the two frames. As compared with the monolithic frame, the lower post-yielding stiffness of the PTSC frame leads to larger deformations and more significant damage to the columns. Besides, the PT tendons elongate with the gaps widening, causing an increase in the PT force, which accelerates the local compression failure at beam ends. The LM values of the two frames are summarized in Table 1.

Due to the scarce literature and experimental data on the definition of LSs in terms of the RDs, three tentative values of LR are used. Because the residual drift of a structure is minimal when it is in elastic stage, LR_1 is defined to be 0.01%. LR_2 is specified to be 10 times of LR_1, i.e., 0.1%, illustrating a medium damage state. McCormick *et al.* (2008) suggested that the permissible residual deformation can be specified to be 0.5% considering the functionality, construction tolerances and safety, hence 0.5% is adopted to define LR_3 herein. The definition of LRs is assumed to be identical for the two frames. It should be emphasized that collapse could lead to a destructive impact on the structure and the consideration of RD in the collapse damage state is insignificant. Therefore, only the maximum deformation (LM_4) is employed to represent the collapse state of the two frame structures. The defined DSs based on the bivariate LSs are shown in Table 2.

4.2 Inputs of seismic ground motions

To conduct the seismic fragility analyses, 30 ground motion records are selected from the PEER-NGA database (https://ngawest2.berkeley.edu/) to be compatible with the response spectrum defined in the Chinese code for seismic design of buildings (National Standards of the People's Republic of China 2010b). The response spectra with 5% damping ratio of the selected ground motions are shown in Fig. 6 along with the code spectrum. Good agreement between the average response spectrum of the selected motions and the target code spectrum can be observed.

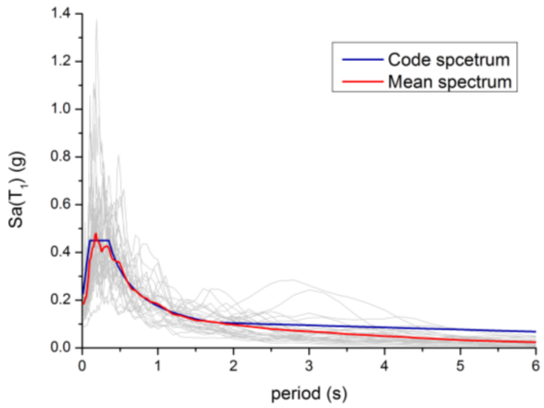

Fig. 6 Response spectra of the selected records and the code spectrum

As discussed above, Incremental Dynamic Analyses (IDA) is performed to generate the seismic fragility curves. According to previous studies (Vamvatsikos and Cornell 2002, Ellingwood *et al.* 2007), the spectral acceleration at the structural fundamental period $S_a(T_1)$ produces a lower dispersion over the full range of EDP values as compared with PGA. This implies that a smaller sample of records is required to estimate median EDP versus IM. Therefore, $S_a(T_1)$ is adopted as the IM in the seismic fragility analyses. The $S_a(T_1)$ values of the selected earthquake records are scaled from 0.1 g to 1.5 g with an increment of 0.1 g. The MDs and RDs of the PTSC and monolithic frames are calculated under each IM level of the 30 ground motion records. The dynamic analyses of the structures are conducted with a Rayleigh damping ratio of 5% for both frames and the Newmark algorithm is adopted to calculate the nonlinear seismic responses. The free vibration with duration of 20s is added to each input ground motion to make the frame come to rest and yield realistic RD. After the nonlinear time history analyses, the seismic fragility curves of the two frame structures are constructed using the methodology presented in Section 2.

5. Results and discussions

5.1 Structural seismic responses

The top displacement time history curves of the monolithic frame and PTSC frame subjected to the Kakogawa record from the Kobe earthquake at $S_a(T_1)$ of 0.2 g, 0.5 g, and 1.0 g are shown in Fig. 7, and Fig. 8 shows the corresponding base shear time history curves. It can be seen that the maximum response of PTSC frame is smaller than that of the monolithic frame at $S_a(T_1)$=0.2 g due to the higher initial stiffness, and the RDs of both frames are negligible. With the increase of IM, the MDs of PTST frame is gradually higher than those of the monolithic frame, while the RDs of the monolithic frame become obviously higher as compared with the PTSC frame. As shown in Fig. 8, no larger base shear is sustained by the PTSC frame than the monolithic counterpart at each IM

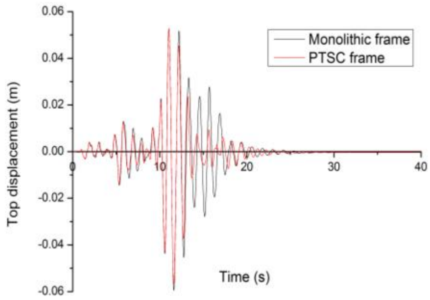

(a)

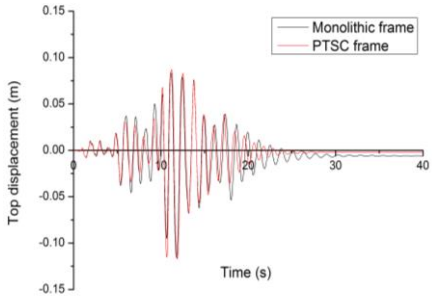

(b)

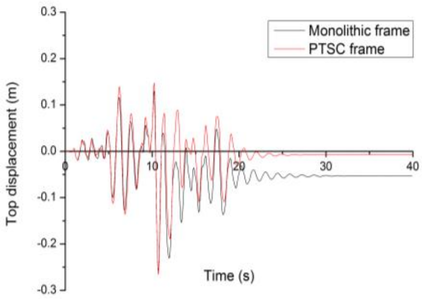

(c)

Fig. 7 Top displacement curves of the Kakogawa record at: (a) 0.2 g, (b) 0.5 g, and (c) 1.0 g

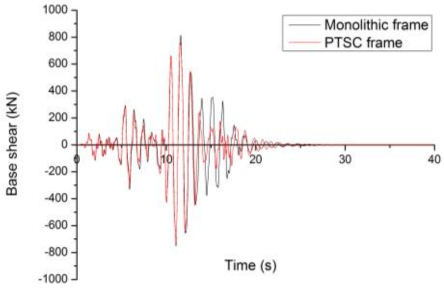

(a)

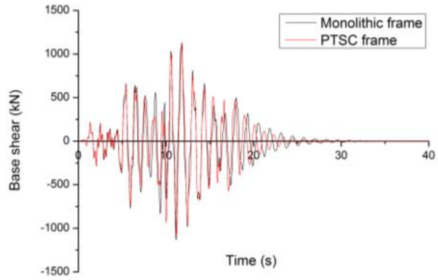

(b)

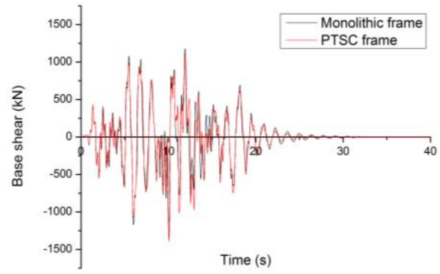

(c)

Fig. 8 Base shear curves of the Kakogawa record at: (a) 0.2 g, (b) 0.5 g, and (c) 1.0 g

level. Therefore, it can be concluded that the deterioration of stiffness of the PTSC frame leads to an extensive displacement response as compared with the monolithic frame. Moreover, the PTSC frame surpasses the monolithic frame in eliminating residual deformations after serious earthquake events owing to its superior re-centering capacity.

Fig. 9 plots the distribution of MDs and RDs under the ground motions at $S_a(T_1)$ of 0.2 g, 0.5 g and 1.0 g. Each point represents the result of a time history analysis with respect to MD (x axis) and RD (y axis). Coincident tendency with that illustrated in Fig. 7 can be observed. At lower ground motion intensities, the MDs and RDs of both frames stay in a minor level. With the increase of IM, a continuous increase of RD with a large dispersion can be observed for the monolithic frame; and the PTSC frame generally experiences slightly larger MDs but smaller RDs as compared to the monolithic frame.

5.2 Joint seismic fragility curves

Fig. 10 shows the fragility curves of the monolithic and PTSC frame with respect to various DSs defined by the bivariant LSs. For general application, the fragility curves are obtained by fitting the probability values with a lognormal cumulative distribution function. However, for the purpose of direct comparisons, the actual data with linear interpolation are plotted to avoid the difference masked by regression smoothing. It can be seen form Fig. 10(a) that for the monolithic frame, the probability of reaching DS_{31} is higher than that of DS_{22}. This illustrates that, even though defined by a larger LM, DS_{31} is a lower damage state compared to DS_{22} for the chosen structure. For the PTSC frame, a distinct overlap of the fragility curves of different DSs can be observed in Fig. 10(b), i.e., the fragility curves of DS_{32} and DS_{33}. Note that the equivalency of fragility corresponds to the same LM. The consistency indicates that the probability for the PTSC frame to sustain the residual drifts in the range LR_2-LR_3 is 0 when suffering from the maximum drifts larger than LM_3. In other words, the residual drifts of the PTSC frame are less than 0.1% (LR_2) when subjected to the selected ground motions at all the IM levels, given that the structure does not collapse.

Comparison of fragility curves for the two frames are shown in Fig. 11, in which M and PT represent the

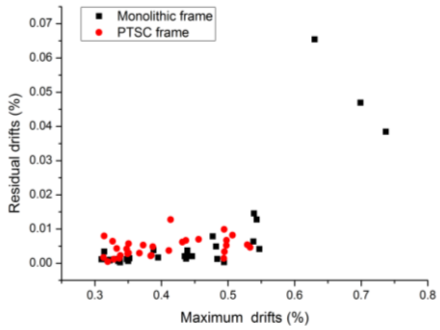

(a)

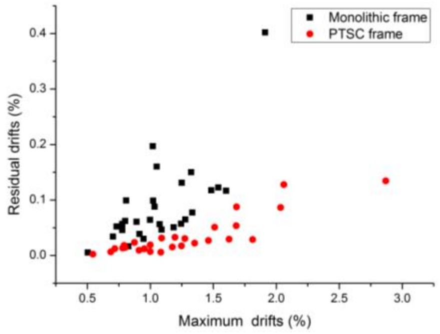

(b)

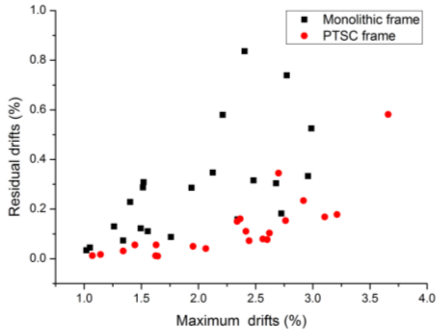

(c)

Fig. 9 Distribution plots of MDs and RDs at: (a) 0.2 g, (b) 0.5 g, and (c) 1.0 g

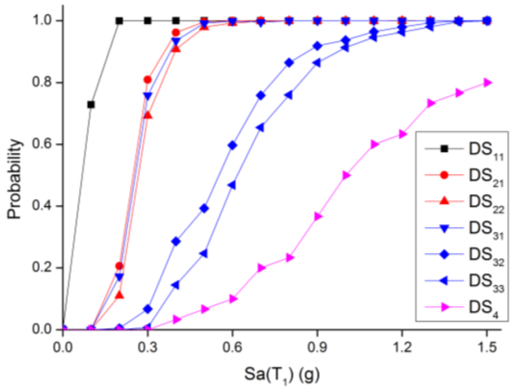

(a)

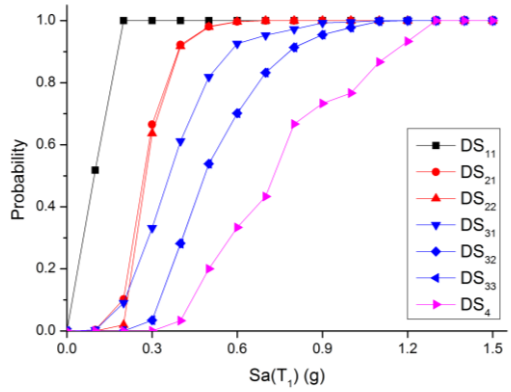

(b)

Fig. 10 Joint fragility curves for (a) the monolithic frame and (b) the PTSC frame

monolithic frame and PTSC frame, respectively. In order to make an explicit presentation of the relatively slight difference among the fragility of lower DS levels, the probabilities of attaining DSs corresponding to LM_1 and LM_2 are extracted and shown in Fig. 11(a). Because all the probabilities grow into unity before the IM reaches 0.8 g, the curves are truncated at $S_a(T_1)$ of 0.8 g. Fig. 11(b) plots the fragility curves of DSs with respect to LM_3 and LM_4.

As shown in Fig. 11(a), the probability of attaining every DS for the monolithic frame is higher than that for the PTSC frame. The seismic fragility in terms of DS_{22} for the monolithic frame is even higher than that of DS_{21} for the PTSC frame. As explained above, the PTSC frame has a higher initial stiffness than the monolithic frame. At lower IM levels, gap opening does not occur at the beam-to-column joints, the frame deforms as rigid bodies. The performance of the PTSC frame is superior to the monolithic frame with respect to both MD and RD at this stage. On the other hand, due to the rigorous deformation limits of these DSs, they are easy to reach under large ground motion inputs, making their fragilities for both frames unity at IMs larger than 0.8 g. Based on the discussions above, the monolithic frame is more vulnerable to suffer slight or moderate damage (expressed as lower DS levels) compared to the PTSC frame.

For the DSs corresponding to LM_3 and LM_4, as illustrated in Fig. 11(b), the seismic fragility of DS_{31} for the monolithic frame is higher than that for the PTSC frame. However, the probabilities for the PTSC frame to attain damage states above DS_{31} are higher than those for the monolithic counterpart. The gap grows with the seriousness of damage states and a much higher collapse fragility for the PTSC frame is observed. In addition, there is a point of intersection between the fragility curves of the two frames. The fragility of DS_{32} for the PTSC frame exceeds that of DS_{32} for the monolithic frame after $S_a(T_1)$ reaches 0.4 g. These observations indicate that, when it comes to serious and destructive damage states, the PTSC frame performs better only in surviving the DSs defined by lower LR values, this superiority is weakened when the ground motion intensity becomes higher. Besides, as larger RDs are permitted, the monolithic frame surpasses the PTSC frame in a synthetical evaluation of seismic performance.

The probability of attaining DS_{ij} can be obtained as the summation of three complementary components: the probability of exceeding the maximum drifts but not reaching the residual drifts (MD > LM_i, RD < LR_j), the probability of exceeding the residual drifts without reaching

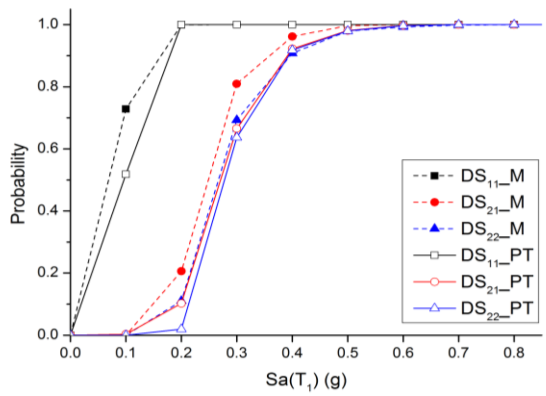

(a)

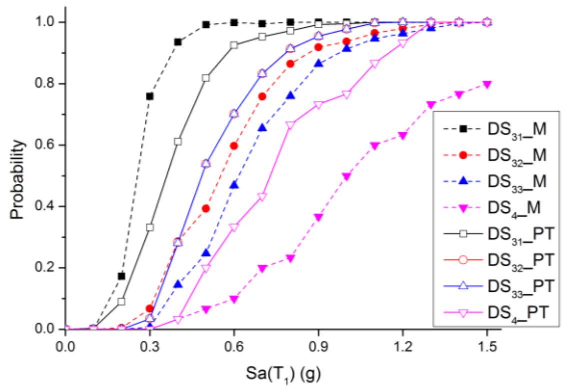

(b)

Fig. 11 Comparison of joint fragility curves for the monolithic frame and PTSC frame corresponding to: (a) LM_1 and LM_2 and (b) LM_3 and LM_4

the maximum drifts (MD < LM_i, RD > LR_j), and the probability of exceeding both limit states (MD > LM_i, RD > LR_j). In order to provide an insight into the contribution of each part, fragilities of DS_{21}, DS_{31}, DS_{32} are disaggregated into above mentioned three probability components, as illustrated in Fig. 12. The corresponding fragility curves are presented in the same figure. Distinctly different trends in the responses of the two frames can be observed. For DS_{21}, the monolithic frame is more inclined to exceed both limit states as compared to the PTSC frame (implied by the larger area of the blue blocks). Although the PTSC frame also responses in larger MDs than LM_2 under most ground motion intensities, its RDs present larger probabilities to stay within LR_1 under lower IM levels (expressed as the yellow block in Fig. 12(a)). The superior ability in controlling RDs of the PTSC frame is further confirmed by Fig. 12(b). However, when it comes to DS_{32} in Fig. 12(c), the higher MDs become the governing response of the PTSC frame that result in the higher joint fragility as compared with the monolithic frame, no matter LR_2 is exceeded or not.

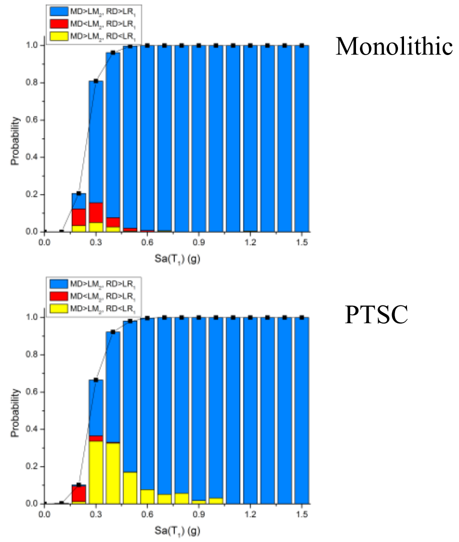

(a)

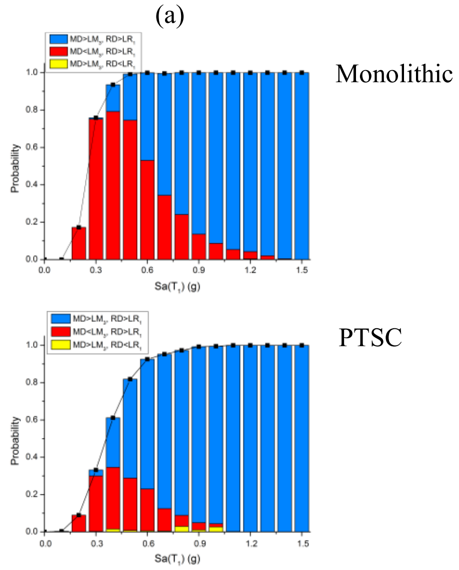

(b)

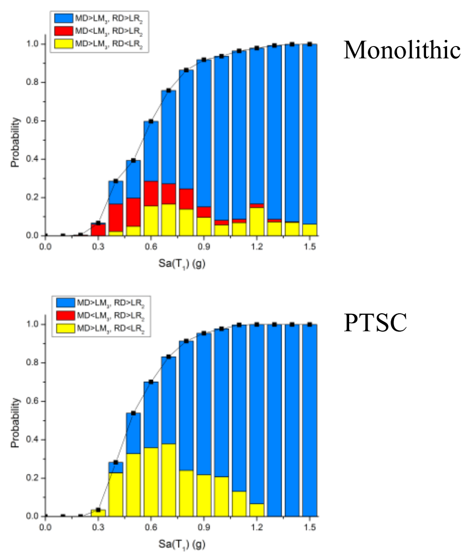

(c)

Fig. 12 Components of the joint fragility for monolithic frame and PTSC frame with respect to (a) DS_{21}, (b) DS_{31}, and (c) DS_{32}

5. Conclusions

In this study, the joint seismic fragility analyses considering the maximum and residual deformations are performed on a PTSC reinforced concrete frame and a conventional monolithic frame. Structural configurations and design criteria of the two frames are identical to make a direct comparison. Based on the numerical results, the following conclusions are drawn:

1. The PTSC frame has a larger initial stiffness but lower post-yield stiffness than the corresponding monolithic frame.
2. Considering maximum and residual deformations simultaneously, the joint fragility for the PTSC frame is lower than the monolithic frame at slight and medium damage states. Nevertheless, the PTSC frame is more vulnerable to suffer severe damage or collapse under large earthquake events.
3. According to the investigation of three probability components of the joint fragility, the superior capacity in eliminating RDs gives the PTSC frame an advantage over the monolithic counterpart in resisting lower DSs. However, with the increase of ground motion intensities, larger MDs of the PTST frame become the dominate factors that result in higher joint fragilities.
4. Neglecting either MD or RD cannot provide reasonable seismic performance assessments of the studied two types of frame structures, especially for the PTSC frame. The proposed seismic fragility analysis method with inclusion of both MD and RD can provide vital support for the performance-based seismic design of PTSC frame structures.

Future research works should be carried out on the appropriate definition of RD performance levels and the judgment of uncertainties associated with RDs, which is beneficial for achieving a more reasonable seismic fragility prediction of PTSC frame structures. Moreover, according to the present research, a key point to improve the seismic performance of the PTSC frame is to enhance its capability to resist strong earthquake ground motions. The further research is expected to focus on the improvement of the structural energy dissipation to reduce maximum deformations, and the proposal of methods to alleviate the seismic damage at the beam and column ends of PTSC frames.

Acknowledgments

The authors would like to acknowledge the financial support from the National Key R&D Program of China (Grant No. 2016YFC0701108) and the National Natural Science Foundation of China (Grant No. 51738007, 51808099) for carrying out this research.

References

ACI Innovation Task Group 1 (2001), *Acceptance Criteria for Moment Frames Based on Structural Testing (T1.1–01) and Commentary (T1.1R-01)*, American Concrete Institute, Farmington Hills, Michigan, U.S.A.

Applied Technology Council (ATC) (1996), *Seismic Evaluation and Retrofit of Concrete Buildings*, Volumes 1 and 2, Report No. ATC-40, Redwood City, California, U.S.A.

ATC (2000), *Prestandard and Commentary for the Seismic Rehabilitation of Buildings*, FEMA 356, Federal Emergency Management Agency, Washington, U.S.A.

ATC, NEHRP (1997), *Guidelines for the Seismic Rehabilitation of Buildings*, FEMA 273, Federal Emergency Management Agency, Washington, U.S.A.

Borekci, M. and Kircil, M.S. (2011), "Fragility analysis of R/C frame buildings based on different types of hysteretic model", *Struct. Eng. Mech.*, **39**(6), 795-812.

Cheok, G.S. and Lew, H.S. (1991), "Model precast concrete beam-to-column connections subject to cyclic loading", *PCI J.*, **36**(3), 56-67.

Chou C.C. and Chen, J.H. (2011), "Seismic design and shake table tests of a steel post-tensioned self-centering moment frame with a slab accommodating frame expansion", *Earthq. Eng. Struct. Dyn.*, **40**(11), 1241-1261.

Chou, C.C. and Chen, J. H. (2010), "Tests and analyses of a full-scale post-tensioned RCS frame subassembly", *J. Constr. Steel Res.*, **66**(11), 1354-1365.

Chou, C.C., Chen, J.H. and Chen, Y.C. (2006), "Evaluating performance of post-tensioned steel connections with strands and reduced flange plates", *Earthq. Eng. Struct. Dyn.*, **35**(9), 1167-1185.

Christopoulos, C., Filiatrault, A. and Uang, C.M. (2002), "Posttensioned energy dissipating connections for moment-resisting steel frames", *J. Struct. Eng.*, **128**(9), 1111-1120.

Christopoulos, C., Pampanin, S. and Priestley, M.J.N. (2003), "Performance-based seismic response of frame structures including residual deformations. Part I: Single-degree of freedom systems", *J. Earthq. Eng.*, **7**(1), 97-118.

Cornell, C.A. and Krawinkler, H. (2000), "Progress and challenges in seismic performance assessment", *Peer Center News*, **20**(2), 130-139.

Cui, Y., Lu, X.L. and Jiang, C. (2017), "Experimental investigation of tri-axial self-centering reinforced concrete frame structures through shaking table tests", *Eng. Struct.*, **132**, 684-694.

Eguchi, R.T., Goltz, J.D., Taylor, C.E., Chang, S.E., Flores, P.J., Johnson, L.A., Seligson, H.A. and Blais N.C. (1998), "Direct economic losses in the northridge earthquake: a three-year post", *Earthq. Spectr.*, **14**(2), 245-264.

El-Sheikh, M., Sause, R., Pessiki, S. and Lu, L.W. (1999), "Seismic behavior and design of unbonded post-tensioned precast concrete frames", *PCI J.*, **44**(3), 54-71.

Ellingwood, B.R., Celik, O.C. and Kinali, K. (2007), "Fragility assessment of building structural systems in Mid-America", *Earthq. Eng. Struct. Dyn.*, **36**(13), 1935-1952.

Elnashait, A.S., Borzi, B. and Viachost, S. (2004), "Deformation-based vulnerability functions for RC bridges", *Struct. Eng. Mech.*, **17**(2), 215-244.

Erberik, M.A. and Elnashai, A.S. (2004), "Fragility analysis of flat-slab structures", *Eng. Struct.*, **26**(7), 937-948.

Fang, C., Zhong, Q., Wang, W., Hu, S. and Qiu, C. (2018), "Peak and residual responses of steel moment-resisting and braced frames under pulse-like near-fault earthquakes", *Eng. Struct.*, **177**, 579-597.

Garlock, M.M. (2005), "Experimental studies of full-scale posttensioned steel connections", *J. Struct. Eng.*, **131**(3), 438-448.

Garlock, M.M., Sause, R. and Ricles, J.M. (2007), "Behavior and design of posttensioned steel frame systems", *J. Struct. Eng.*, **133**(3), 389-399.

GB 50010-2010 (2010a), *Code for Design of Concrete Structures, National Standards of the People's Republic of China*, Beijing, China.

GB 50011-2010 (2010b), *Code for Seismic Design of Buildings*, National Standards of the People's Republic of China, Beijing,

China.
Ghosh, S.K. and Cleland, N. (2012), “Observations from the February 27, 2010, earthquake in Chile”, *PCI J*., **57**(1), 52-75.
Guo, T., Song, L.L. and Cao, Z. (2016), “Large-scale tests on cyclic behavior of self-centering prestressed concrete frames”, *ACI Struct. J*., **113**(6), 1263-1274.
Guo,T., Song, L.L. and Zhang, G.D. (2015), “Numerical Simulation and seismic fragility analysis of a self-centering steel MRF with web friction devices”, *J. Earthq. Eng*., **19**(5), 731-751.
Kammula, V., Erochko, J. and Kwon, O.S. (2014), “Application of hybrid-simulation to fragility assessment of the telescoping self-centering energy dissipative bracing system”, *Earthq. Eng. Struct. Dyn*., **43**(6), 811-830.
Kang, J.W. and Lee, J. (2016), “A new damage index for seismic fragility analysis of reinforced concrete columns”, *Struct. Eng. Mech*., **60**(5), 875-890.
Kim, H.J. and Christopoulos, C. (2009), “Numerical models and ductile ultimate deformation response of post-tensioned self-centering moment connections”, *Earthq. Eng. Struct. Dyn*., **38**(1), 1-21.
Kwon, O.S. and Elnashai, A. (2006), “The effect of material and ground motion uncertainty on the seismic vulnerability curves of RC structure”, *Eng. Struct*., **28**(2), 289-303.
Li, C., Hao, H., Li, H.N. and Bi, K.M. (2016), “Seismic fragility analysis of reinforced concrete bridges with chloride induced corrosion subjected to spatially varying ground motions”, *Int. J. Struct. Stab. Dyn*., **16**(5), 1550010.
Li, C., Li, H.N., Hao, H., Bi, K.M. and Chen, B.K. (2018), “Seismic fragility analyses of sea-crossing cable-stayed bridges subjected to multi-support ground motions on offshore sites”, *Eng. Struct*., **165**, 441-456.
Lin, Y.C., Sause, R. and Ricles, J. (2013a), “Seismic performance of a large-scale steel self-centering moment-resisting frame: MCE hybrid simulations and quasi-static pushover tests”, *J. Struct. Eng*., **139**(7), 1227-1236.
Lin, Y.C., Sause, R. and Ricles, J. (2013b). “Seismic performance of steel self-centering, moment-resisting frame: Hybrid simulations under design basis earthquake”, *J. Struct. Eng*., **139**(11), 1823-1832.
Lu, X.L., Cui, Y., Liu, J.J. and Gao, W.J. (2015), “Shaking table test and numerical simulation of a 1/2-scale self-centering reinforced concrete frame”, *Earthq. Eng. Struct. Dyn*., **44**(12), 1899-1917.
Luco, N., Bazzurro, P. and Cornell, C.A. (2004), “Dynamic versus static computation of the residual capacity of a main shock damaged building to withstand an aftershock”, *Proceedings of the 13th WCEE*, Vancouver, B.C., Canada.
Mackie, K. and Stojadinovic, B. (2004), “Residual displacement and post earthquake capacity of highway bridges”, *Proceedings of the 13th WCEE*, Vancouver, B.C., Canada.
McCormick, J., Aburano, H., Ikenaga, M. and Nakashima, M. (2008), “Permissible residual deformation levels for building structures considering both safety and human elements”, *Proceedings of the 14th WCEE*, Beijing, China.
Mckenna, F. and Fenves, G.L. (2013), *Open System for Earthquake Engineering Simulation (OpenSees)*, Pacific Earthquake Engineering Research Center, University of California, U.S.A.
Morgen, B.G. and Kurama, Y. C. (2004), “A friction damper for post-tensioned precast concrete moment frames”, *PCI J*., **49**(4), 112-133.
Morgen, B.G. and Kurama, Y.C. (2007), “Seismic design of friction-damped precast concrete frame structures”, *J. Struct. Eng*., **133**(11), 1501-1511.
Morgen, B.G. and Kurama, Y.C. (2008), “Seismic response evaluation of posttensioned precast concrete frames with friction dampers”, *J. Struct. Eng*., **134**(1), 132-145.
Muguruma, H., Nishiyama, M. and Watanabe, F. (1995), “Lessons learned from the Kobe Earthquake: A Japanese Perspective”, *Pci J*., **40**(4), 28-42.
Nakaki, S.D. and Englekirk, R.E. (1991), “PRESSS industry seismic workshops: Concept development”, *PCI J*., **36**(6), 54-61.
New Zealand Standards (NZS) (2006), *Concrete Design Standard*, NZS 3101:2006, Wellington, New Zealand.
Pampanin, S., Christopoulos, C. and Priestley, M.J.N. (2002), *Residual Deformations in the Performance Based Seismic Assessment of Frame Structures*, Report ROSE-2002/02, European School for Advanced Studies in Reduction of Seismic Risk, University of Pavia, Italy.
Pampanin, S., Christopoulos, C. and Priestley, M.J.N. (2003), “Performance-based seismic response of frame structures including residual deformations. Part II: Multi-degree of freedom systems”, *J. Earthq. Eng*., **7**(1), 119-147.
Priestley, M.J.N. (1991), “Overview of PRESSS research program”, *PCI J*., **36**(4), 50-57.
Priestley, M.J.N. and Macrae, G.A. (1996), “Seismic tests of precast beam-to-column joint subassemblages with unbonded tendons”, *PCI J*., **41**(1), 64-81.
Qiu, C. and Zhu, S. (2017), “Shake table test and numerical study of self-centering steel frame with SMA braces”, *Earthq. Eng. Struct. Dyn*., **46**(1), 117-137.
Rahgozar, N., Moghadam, A.S. and Aziminejad, A. (2017), “Response of self-centering braced frame to near-field pulse-like ground motions”, *Struct. Eng. Mech*., **62**(4), 497-506.
Roh, H. and Reinhorn, A.M. (2009), “Analytical modeling of rocking elements”, *Eng. Struct*., **31**(5), 1179-1189.
Rosenblueth, E. and Meli, R. (1986), “The 1985 Mexico earthquake: Causes and effects in Mexico City”, *Concrete Int. (ACI)*, **8**(5), 23-34.
Rota, M., Penna, A. and Magenes, G. (2010), “A methodology for deriving analytical fragility curves for masonry buildings based on stochastic nonlinear analyses”, *Eng. Struct*., **32**(5), 1312-1323.
Saatcioglu, M., Mitchell, D., Tinawi, R., Gardner, N.J., Gillies, A.G., Ghobarah, A., Anderson, D.L and Lau, D. (2001), “The august 17, 1999, Kocaeli (turkey) earthquake-damage to structure”, *Can. J. Civil Eng*., **28**(4), 715-737.
Shen, J. and Astaneh-Asl, A. (2000), “Hysteresis model of bolted-angle connections”, *J. Constr. Steel Res*., **54**(3), 317-343.
Shrestha,B., Li, C. and Hao, H. (2016), “Performance-based seismic assessment of superelastic shape memory alloy-reinforced bridge piers considering residual deformations”, *J. Earthq. Eng*., **21**(7), 1050-1069.
Song, L.L. (2016), “Seismic performance and design method of self-centering concrete frames”, Ph.D. Dissertation, Southeast University, Nanjing, China.
Song, L.L., Guo, T. and Chen, C. (2014), “Experimental and numerical study of a self-centering prestressed concrete moment resisting frame connection with bolted web friction devices”, *Earthq. Eng. Struct. Dyn*., **43**(4), 529-545.
Stanton, J. (1997), “A hybrid reinforced precast frame for seismic region”, *PCI J*., **42**(2), 20-23.
Tian, L. and Qiu, C. (2018), “Modal pushover analysis of self-centering concentrically braced frames”, *Struct. Eng. Mech*., **65**(3), 251-261.
Uma, S.R., Pampanin, S. and Christopoulos, C. (2010), “Development of probabilistic framework for performance-based seismic assessment of structures considering residual deformations”, *J. Earthq. Eng*., **14**(7), 1092-1111.
Vamvatsikos, D. and Cornell, C.A. (2002), “Incremental dynamic analysis”, *Earthq. Eng. Struct. Dyn*., **31**(3), 491-514.
Waseem, M. and Spacone, E. (2017), “Fragility curves for the

typical multi-span simply supported bridges in northern pakistan", *Struct*. *Eng*. *Mech*., **64**(2), 213-223.

Zhang, A.L., Zhang, Y.X., Li, R. and Wang, Z. Y. (2016), "Cyclic behavior of a prefabricated self-centering beam-column connection with a bolted web friction device", *Eng*. *Struct*., **111**, 185-198.

CC